nature mental health

Supplementary information https://doi.org/10.1038/s44220-026-00672-y

Decoding the temporal dynamics of face-specific neural representations in autism

In the format provided by the authors and unedited

Supplementary Information

Robustness of decoding analysis

Impact of IQ

Since NT children had significantly lower IQ scores than autistic children, we ruled out the possibility that our primary findings were driven my differences in IQ scores. On average, there was a statistically significant association between IQ and decoding accuracy in both autistic and NT children. However, we found that this association was moderated by the time window selected. For example, for mean decoding accuracy from 200-500ms there was a significant association but not for the time window of 0-250ms, an important theoretical time window for face processing.

Data/Signal Quality

Number of Accepted Trials

Table SI1. Mean number of accepted trials in each age group and diagnostic group.

Condition	Group	6-7 years	8-9 years	10-11 years	Group difference?	Age Difference?	Group x Age Interaction
Image	Autism	13.65	15.3	16.33	p = .03	$p = 3 \times 10^{-6}$	$p = .72$
Image	NT	14.94	15.97	17.79			
Identity	Autism	13.81	15.86	17.19	p = .001	$p = 4.2 \times 10^{-8}$	$p = .55$
Identity	NT	15.89	16.85	18.92			
Faces	Autism	38.95	44.8	49.13	$p = 7.1 \times 10^{-9}$	$p = 1.5 \times 10^{-7}$	$p = .64$
Faces	NT	49.16	52.04	58.64			
Orientation	Autism	38.77	44.76	50	$p = 1.5 \times 10^{-9}$	$p = 2.0 \times 10^{-8}$	$p = .49$
Orientation	NT	49.98	52.09	59.24			

Note. NT = neurotypical. Comparisons are two-sided F-tests derived from main effects of group (Autistic, NT) or age group (6-7, 8-9, 10-11), and the Group x Age group interaction.

Impact of Data/Signal Quality on Decoding Accuracy

Differences in signal quality or variability between groups can indeed influence decoding performance, particularly in clinical samples. To address this, we quantified trial-to-trial variability using the contrast-to-noise ratio (CNR) following Bae et al. (2020), which isolates noise unrelated to condition, electrode, or interaction effects. First, we found no significant differences in CNR between autistic and neurotypical children across all decoding conditions (see Analysis 1 below). Second, there were no differences across age groups (6–7, 8–9, 10–11 years) for any condition (see Analysis 2 below). Third, CNR did not significantly predict decoding accuracy for any condition (see Analysis 3 below). Finally, these associations were not moderated by age group (see Analysis 4 below), except for an interaction for all images ($p < .05$), where higher CNR in the 8–9-year group was associated with slightly reduced decoding accuracy. Importantly, this effect was not observed for face, orientation, or identity conditions.

Figure SI1. Scatterplots show raw data and fitted regression lines (with 95% confidence Interval ribbons) for decoding accuracy as a function of CNR for each condition.

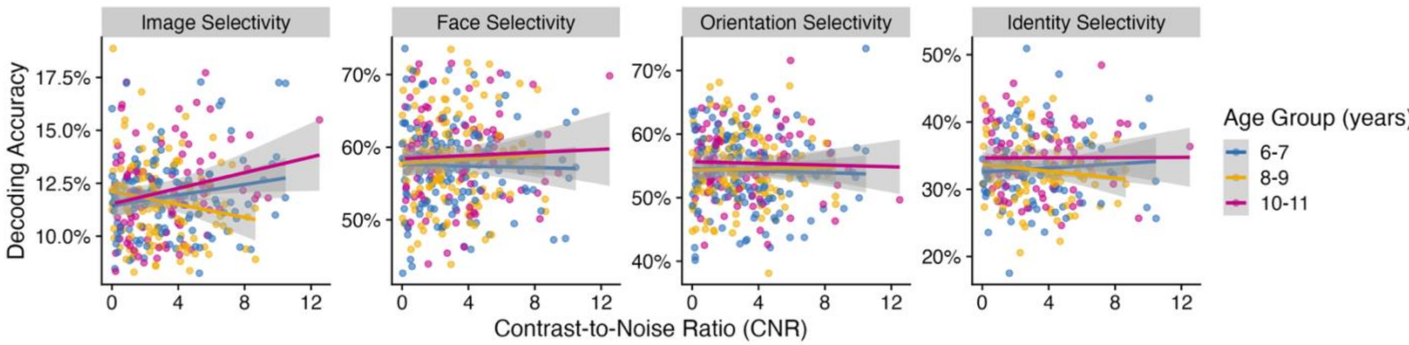

Table SI2. Regression models evaluating differences in CNR and the impact of CNR on decoding accuracy

Analysis	Dependent variable ~ independent variable	All Images	Face	Orientation	Identity
1	CNR ~ group (autism vs. NT)	$p = .79$	$p = .43$	$p = .46$	$p = .94$
2	CNR ~ age group (6-7 vs 8-9 vs. 10-11)	$p = .97$	$p = .56$	$p = .59$	$p = .88$
3	Decoding ~ CNR (Main effect of CNR)	$p = .17$	$p = .93$	$p = .98$	$p = .70$
4	Decoding ~ CNR * age group	$p = .25$	$p = .62$	$p = .74$	$p = .77$

Note. CNR = Contrast to Noise Ratio; NT = neurotypical; Main effects for Analysis 1 and 2 and Interaction effects for Analysis 3 and 4 are derived from linear regression models. Model notation is described in the Table (column 2).

Representation Similarity Analysis

Overall Differences between autistic and neurotypical (NT) children

A permutation approach was computed to compare the overall RDM geometry of the brain among autistic and NT individuals across 9 different stimuli among the three possible conditions. Using the observed data, average RDM mean matrices for autistic and NT, as well as the difference between the two matrices were computed. The Frobenius norm of the difference matrix (i.e., Euclidian norm of a matrix) for the observed data, Δ_{F_0}, was computed.

$$\Delta_{F_0} = \|ASD_0 - NT_0\|_F$$

Ten-thousand permutations (J = 10,000) of the true dataset were then estimated, where participant data was randomly assigned to either the "NT" or "Autistic" groups. To ensure comparability with the observed data, each permutation included n = 109 randomly selected participants in the NT group and n = 249 randomly selected participants in the autistic group, and the Frobenius distance was computed for each permutation, Δ_{F_j}, then averaged across all permutations, Δ_{F_1}.

$$\Delta_{F_j} = \left\|ASD_j - NT_j\right\|_F$$

$$\Delta_{F_1} = \frac{\sum_1^J \Delta_{F_j}}{J}$$

The probability of Δ_F was then computed as an average of the number of times that the permutation statistic was greater than or equal to the observed statistic.

$$p_F = P(\Delta_{F_1} \geq \Delta_{F_0})$$

Results showed that the Frobenius norm of the observed data ($\Delta_{F_0} = 0.643$) was larger than the mean of the permutation data ($\Delta_{F_1} = 0.379$) beyond chance ($p_F < .001$; see Figure SI2).

Figure SI2. Distribution of Permutation Difference Values (Δ_{F_j}) Compared to the Observed Difference Value (Δ_{F_0}) across All Conditions

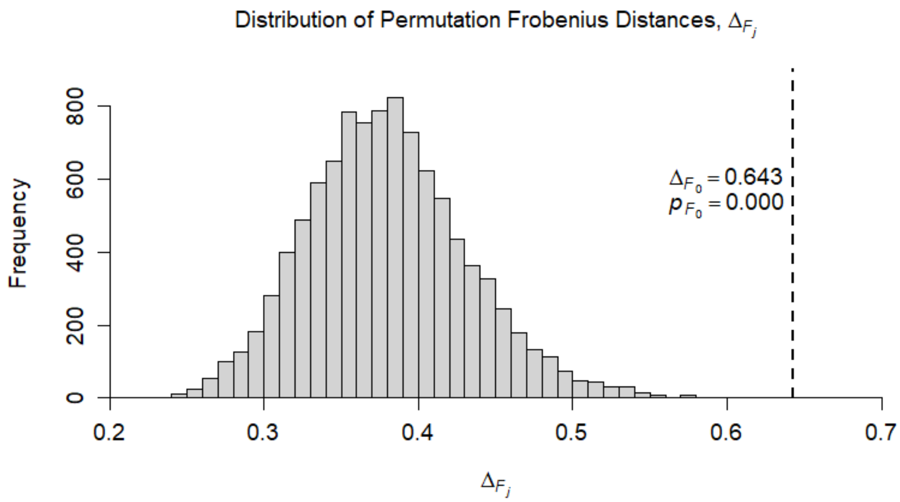

Note. This figure shows the null distribution of Frobenius distances, Δ_{F_j}, computed from 10,000 permutations (graphically represented as a histogram), alongside the Frobenius distance computed from the observed data, Δ_{F_0} (graphically represented as a black dotted line). The probability of the observed value belonging to the null distribution is extremely low, $p_F < .001$.

Differences between autistic and NT children within conditions (Houses, Faces, Inverted Faces)

The permutation approach was further used to compare differences in RDM geometry between autistic and NT groups within conditions. For houses, results showed that the Frobenius norm of the observed data ($\Delta_{F_0} = 0.196$) had a low probability of belonging to the permutation computed null distribution ($p_F = .03$). Results showed the same overall effect for both the upright ($\Delta_{F_0} = 0.203, p_F = .02$) and inverted faces ($\Delta_{F_0} = 0.198, p_F = .02$). Across all conditions, results showed that the observed value was unlikely to fall in the null distribution (see Figure SI2), supporting differences in RDM geometry across autistic and NT over conditions.

Figure SI3.

Distribution of Permutation Difference Values (Δ_{F_j}) Compared to Observed Difference Values (Δ_{F_0}) within House, Face, and Inverted Face Conditions

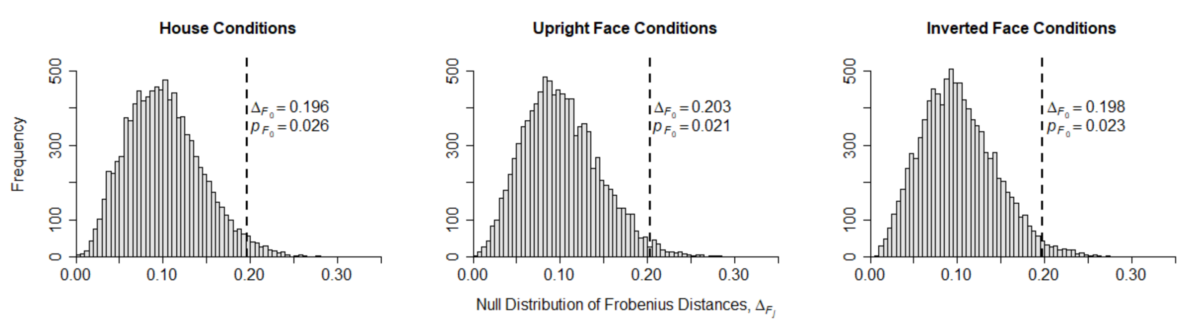

Note. This figure shows the null distributions of Frobenius distances, Δ_{F_j}, computed from 10,000 permutations (graphically represented as a histogram), alongside the Frobenius distances computed from the observed data, Δ_{F_0} (graphically represented as a black dotted line) for each condition. The probability of the observed value belonging to the null distribution is relatively small, $.02 \leq p_F \leq .03$.

Table SI3. Studies reporting atypical activation of brain regions in autism shown in Figure 1 of the main text

Study	Cortical Region	Lobe	Division	Neuroimaging measure
Bookheimer et al. (2008)	Amygdala	Temporal	Subcortical	fMRI
Hazlett et al. (2009)	Amygdala	Temporal	Subcortical	structural
Mosconi et al. (2009)	Amygdala	Temporal	Subcortical	structural
Nordahl et al. (2012)	Amygdala	Temporal	Subcortical	structural
Schumann et al. (2009)	Amygdala	Temporal	Subcortical	structural
Sparks et al. (2002)	Amygdala	Temporal	Subcortical	structural
Ashwin et al. (2007)	Anterior cingulate gyrus	Frontal	Subcortical	fMRI
Redcay et al. (2008)	Anterior cingulate gyrus	Frontal	Subcortical	structural
Hadjikhani	Anterior insula	Temporal	Subcortical	fMRI
Muller et al. (2001)	Basal ganglia	Subcortical	Subcortical	fMRI
Harris et al. (2006)	Broca's area	Temporal	Cortical	fMRI
Vaidya et al. (2011)	Caudate nucleus	Subcortical	Subcortical	fMRI
Hazlett et al. (2009)	Caudate nucleus	subcortical	Subcortical	structural
Qiu et al. (2016)	Caudate nucleus	Subcortical	Subcortical	structural
Akshoomoff et al. (2004)	Cerebellar vermis	Midbrain	Subcortical	structural
Webb et al. (2009)	Cerebellar vermis	Midbrain	Subcortical	structural
Silani et al. (2008)	Cerebellum	Midbrain	Subcortical	fMRI
Akshoomoff et al. (2004)	Cerebellum	Midbrain	Subcortical	structural
Courchesne et al. (2001)	Cerebellum	Midbrain	Subcortical	structural
Wolff et al. (2015)	Corpus Callosum	Midbrain	Subcortical	structural
Wenstein et al. (2011)	Corpus Callosum	Midbrain	Subcortical	structural
Xiao et al. (2014)	Corpus Callosum	Midbrain	Subcortical	structural
Wick et al. (2008)	Dorsolateral prefrontal cortex	Frontal	Cortical	fMRI
Carper et al. (2005)	Dorsolateral prefrontal cortex	Frontal	Cortical	structural
Agam et al. (2010)	Frontal eye field	Frontal	Cortical	fMRI
Corbett et al. (2009)	Frontal gyrus	Frontal	Cortical	fMRI
Hall et al. (2010)	Fusiform gyrus	Temporal	Cortical	fMRI
Hoef et al. (2011)	Fusiform gyrus	Temporal	Cortical	structural
Wenstein et al. (2011)	Corpus Callosum	Midbrain	Subcortical	structural
Hazlett et al. (2009)	Globus pallidus	Subcortical	Subcortical	structural
Schumann	Hippocampus	Temporal	Subcortical	fMRI
Hazlett et al. (2009)	Hippocampus	Temporal	Subcortical	structural
Hall et al. (2003)	Inferior frontal area	Frontal	Cortical	fMRI
Hadjikhani et al. (2007)	Inferior frontal cortex	Frontal	Cortical	fMRI
Bookheimer et al. (2008)	Inferior frontal gyrus	Frontal	Cortical	fMRI
Ogai et al. (2003)	Insula	Temporal	Subcortical	fMRI
Solso et al. (2016)	Internal Capsule	Basal ganglia	Subcortical	structural
Muller et al. (2001)	Ipsilateral cerebellum	Subcortical	Subcortical	fMRI
Dalton et al. (2005)	Medial frontal gyrus	Frontal	Cortical	fMRI
Hubl et al. (2003)	Medial occipital gyrus	Occipital	Cortical	fMRI
Eyler et al. (2012)	Medial occipital gyrus	Occipital	Cortical	structural
Carper et al. (2005)	Medial prefrontal cortex	Frontal	Cortical	structural

Kleinhans et al. (2010)	Middle temporal gyrus	Temporal	Cortical	fMRI
Dichter et al. (2012	Nucleus accumbens	Subcortical	Subcortical	fMRI
Dalton et al. (2005)	Orbitofrontal gyrus	Frontal	Cortical	fMRI
Luna et al. (2002)	Posterior cingulate cortex	Parietal	Cortical	fMRI
Arutiunian et al. (2023)	Precentral gyrus	Parietal	Cortical	structural
Bookheimer et al. (2008)	Precuneus	Parietal	Cortical	fMRI
Kleinhans et al. (2010)	Prefrontal cortex	Frontal	Cortical	fMRI
Hadjikhani et al. (2007)	Premotor cortex	Parietal	Cortical	fMRI
Ogai et al. (2003)	Putamen	Subcortical	Subcortical	fMRI
Hazlett et al. (2009)	Putamen	Subcortical	Subcortical	structural
Weng et al. (2011)	Striatum	Subcortical	Subcortical	fMRI
Loveland et al. (2008)	Superior temporal gyrus	Temporal	Cortical	fMRI
Eyler et al. (2012)	Superior temporal gyrus	Temporal	Cortical	structural
Ashwin et al. (2007)	Superior temporal sulcus	Temporal	Cortical	fMRI
Pitskel et al. (2011)	Temporal parietal junction	Temporal	Cortical	fMRI
Silani et al. (2008)	Temporal pole	Temporal	Cortical	fMRI
Hall et al. (2003)	Thalamus	Subcortical	Subcortical	fMRI
Belmonte et al. (2003)	Inferior occipital gyrus	Occipital	Cortical	fMRI
Hopfinger et al. (2008)	Ventrolateral prefrontal cortex	Frontal	Cortical	fMRI
Monk et al. (2010)	Ventromedial prefrontal cortex	Frontal	Cortical	fMRI
Anderson et al. (2010)	Wernicke's Area	Temporal	Cortical	fMRI